JACC: CARDIOVASCULAR IMAGING
VOL. 3, NO. 11, 2010

ISSN 1936-878X/$36.00
PUBLISHED BY ELSEVIER INC.
DOI:10.1016/j.jcmg.2010.09.011

Use of Angiographic CT Imaging in the Cardiac Catheterization Laboratory for Congenital Heart Disease

Andrew C. Glatz, MD,* Xiaowei Zhu, MS,† Matthew J. Gillespie, MD,*
Brian D. Hanna, MD, PhD,* Jonathan J. Rome, MD*
Philadelphia, Pennsylvania

OBJECTIVES This study sought to retrospectively evaluate our initial experience using angiographic computed tomography (ACT) in a pediatric cardiac catheterization laboratory.

BACKGROUND ACT provides cross-sectional CT images from a rotational angiography run using a C-arm mounted flat-panel detector in the interventional suite. A 3-dimensional (3D) angiographic image can be created from the CT volume set and used in real time during the procedure. To our knowledge, its use has never previously been described for congenital heart disease.

METHODS 3D reconstructions were created and we retrospectively reviewed cases during our first year of ACT use. Images obtained were independently evaluated to determine their diagnostic utility. Radiation dose reduction protocols were defined using phantom testing and radiation dose calculation.

RESULTS ACT was used during 41 cardiac catheterizations in patients at a median age of 5.1 years (range: 0.4 to 58.8 years) for evaluation of: right ventricular outflow tract (RVOT)/central pulmonary arteries (PAs) in 20; cavopulmonary connection (CPC) in 11; pulmonary veins in 5; distal PAs in 4; and other locations in 5. Four subjects had 2 anatomic areas studied by ACT. The mean contrast volume for ACT was 1.2 ± 0.4 ml/kg. Diagnostic-quality imaging was obtained in 71% of cases: 13/20 RVOT/central PAs; 9/11 CPC; 4/5 pulmonary veins; 2/4 distal PAs; and 4/5 others. In 12 cases, ACT contributed to clinical outcomes beyond standard angiography. Radiation dose reduction protocols allowed ACT to be comparable in exposure to a standard biplane cineangiogram.

CONCLUSIONS Diagnostic-quality imaging can be obtained using ACT in 71% of cases without a significant increase in contrast or radiation exposure. In certain cases, ACT provides additional anatomic detail and may aid complex catheter manipulations. Future work is needed to continue to define applications of this new technology. (J Am Coll Cardiol Img 2010;3:1149–57) © 2010 by the American College of Cardiology Foundation

From the *Division of Cardiology, Department of Pediatrics, the Children's Hospital of Philadelphia, University of Pennsylvania School of Medicine, Philadelphia, Pennsylvania; and the †Department of Radiology, the Children's Hospital of Philadelphia, University of Pennsylvania School of Medicine, Philadelphia, Pennsylvania. The authors have reported that they have no relationships to disclose.

Manuscript received April 14, 2010; revised manuscript received August 26, 2010, accepted September 16, 2010.

JACC: CARDIOVASCULAR IMAGING, VOL. 3, NO. 11, 2010
NOVEMBER 2010:1149–57

Angiographic computed tomography (ACT) is a new imaging modality that provides cross-sectional CT images from a rotational angiography run using a C-arm–mounted flat-panel detector. The volume set obtained can be manipulated on a separate workstation in the interventional suite to generate a 3-dimensional (3D) angiographic image combined with CT-quality soft tissue imaging that can be used in real time during the procedure. Designed originally for use in interventional neurovascular procedures (1–8), its use has extended into other interventional radiology realms, including abdominal (9–11), spine (12), and hepatic vascular (13–18). Its application outside interventional radiology is quite limited. Noelker et al. (19) reported the use of ACT for mapping of the left atrium during atrial fibrillation ablation procedures. There have also been early reports of its use in adult thoracic vascular interventions (20). To our knowledge, the use of ACT for patients with congenital heart disease has never previously been described. We describe our initial experience using ACT in a pediatric cardiac catheterization laboratory.

ABBREVIATIONS AND ACRONYMS

3D = 3-dimensional

ACT = angiographic computed tomography

CMR = cardiac magnetic resonance

CPC = cavopulmonary connection(s)

MSCT = multislice computed tomography

PA = pulmonary artery

RVOT = right ventricular outflow tract

METHODS

This study was conducted with approval from our Institutional Review Board (IRB # 2009-1-6377). Where appropriate, informed consent was obtained.

Case review. A retrospective review was performed of all cases from our cardiac catheterization laboratory, which utilized ACT between July 1, 2008, and June 30, 2009. Identified cases were reviewed for demographic, clinical, and procedural details. ACT images obtained were reanalyzed and compared with standard cineangiographic images to determine cases where ACT provided diagnostic-quality information. The reviewer was blinded to the demographic and clinical details of the case. As much as practically possible, the reviewer was also unaware of the clinical outcome of the case. Diagnostic-quality information is subjectively defined as being equivalent to the information obtained (or expected to be obtained) by traditional 2-dimensional projectional cineangiography. Further, cases were identified in which ACT provided additional clinically relevant information.

Image acquisition and processing. ACT images were acquired using a C-arm–mounted flat-panel biplane angiographic system (Artis zee, Siemens Medical Solutions, Forchheim, Germany) using commercially available software (syngo DynaCT, Siemens Medical Solutions). Post-processing was performed on a separate workstation in the interventional suite (Leonardo, Siemens Medical Solutions). ACT data acquisition was performed with the following parameters: 190° rotation, 5-s ungated acquisition time, projection on either 20-cm × 20-cm or 30-cm × 40-cm flat-panel detector size, 48-cm field of view. We displayed the tomographic volume set at a slice thickness of 0.3 mm, although this is adjustable during post-processing. The degree of thresholding during 3D image reconstruction was determined by the operator to optimize image quality. For patients mechanically ventilated during the catheterization, ventilation was held during the period of image acquisition. In awake patients, spontaneous breath-holding was performed when possible. Radiation dose programs were modified from the installation settings in order to minimize radiation exposure while maintaining image quality. Intravenous contrast media (Ioversol 74% [350 mg/ml], Optiray, Covidien Imaging Solutions, Hazelwood, Missouri) was diluted 1:2. Contrast volumes were weight-based and administered with a 0.5- to 5-s X-ray delay based on the clinical situation.

Radiation dose testing. Radiation dose testing was performed using radiologic phantoms (ATOM, Computerized Imaging Reference Systems, Inc., Norfolk, Virginia) utilizing 6 different available ungated cardiac ACT acquisition programs across a range of dose/frame and frame rates. The dose-area product as measured by the Artis zee system (Siemens Medical Solutions) during phantom testing for each program was converted to an estimated total effective dose (mSv) using the Monte Carlo method on commercially available software (PCXMC v2.0, STUK, Helsinki, Finland). For comparative purposes, radiation exposure from standard fluoroscopy and biplane cineangiography was also measured.

Statistical methods. Summary data are presented as frequency with percentage of total for count data, median with range for non-normally distributed continuous variables, and mean with standard deviation for normally distributed continuous variables. Difference in the frequency of diagnostic-quality images obtained by ACT across anatomic categories was assessed using Pearson chi-square. Logistic regression was used to attempt to identify demographic, clinical, or procedural variables associated with obtaining diagnostic-quality images. Statistical significance was established at $p < 0.05$. All statistical analyses were performed using STATA version 10 (StataCorp LP, College Station, Texas).

RESULTS

Case review. Between July 1, 2008, and June 30, 2009, 1,083 total cases were performed in our cardiac catheterization laboratory, of which 705 were diagnostic and/or interventional cases utilizing angiography. Of these, ACT was utilized in 41 (5.8%), of which 12 were diagnostic and 29 were interventional. Demographic, clinical, and procedural details of the reviewed cases are summarized in Table 1. ACT was used across a wide range of patient ages, sizes, and total fluoroscopy times, reflective of the range of case complexity in which ACT was utilized. ACT was performed with breath-holding in a total of 32 cases (78%): 25 were with ventilator-hold in an anesthetized and intubated patient, and 7 were with the patient awake and able to perform spontaneous breath-hold during the 5 s of image acquisition. In 9 cases, ACT was performed with a patient under conscious sedation, but too young to cooperate with spontaneous breath-hold. In all of these 9 cases, we were imaging central structures, and respiratory movements did not significantly interfere with image quality. Total contrast administered was within the acceptable range, with the volume used for ACT constituting, on average, 35% of the total contrast load. Patients were classified into 5 anatomic categories based on the region of interest for visualization by ACT. There were 4 cases in which ACT was used to assess 2 different anatomic regions, so these 4 patients counted for 2 different categories. Anatomic categories consisted of the following:

Table 1. Summary of Clinical and Procedural Details of Procedures Utilizing ACT (n = 41)

Sex, male	20 (49%)
Age, yrs	5.1 (0.4–58.8)
Height, cm	107 (60–173)
Weight, kg	19.8 (5.0–114.4)
Body surface area, kg/m^2	0.73 (0.28–2.21)
Heart rate, beats/min	96.9 ± 28.7
Fluoroscopy time, min	29.8 (1.7–134.3)
No. of standard cineangiograms/case	8 (0–20)
Total contrast/wt, ml/kg	4.0 ± 1.6
ACT contrast/wt, ml/kg	1.2 ± 0.4
ACT contrast as % of total	35 ± 16
Anatomic category*	
Reconstructed RVOT/central pulmonary arteries	20 (49%)
Cavopulmonary connection	11 (27%)
Pulmonary veins	5 (12%)
Distal pulmonary arteries	4 (10%)
Other	5 (12%)

Results expressed as number (with percentage of total), median (with range), or mean ± standard deviation. *Four subjects assigned to 2 different anatomic categories.
ACT = angiographic computed tomography; RVOT = right ventricular outflow tract; wt = weight.

THE RECONSTRUCTED RIGHT VENTRICULAR OUTFLOW TRACT AND CENTRAL PULMONARY ARTERIES. There were 20 procedures performed in patients at a median age of 3.5 years (range 0.4 to 58.8 years) and weight of 18.7 kg (range 5.1 to 74 kg). These patients had undergone surgical repair of tetralogy of Fallot (n = 8), truncus arteriosus (n = 4), double outlet right ventricle (n = 4), or d-transposition of the great arteries (n = 3); 1 had undergone a Ross-Kono procedure. The median fluoroscopy time was 29.4 min (range 11.3 to 134.3 min) with a mean total case contrast volume of 4.2 ± 1.3 ml/kg and mean contrast volume for ACT of 1.3 ± 0.4 ml/kg. During ACT, contrast was injected either into the right ventricle (n = 11) or right ventricular outflow tract (RVOT) (n = 9) with an X-ray delay of 1 s. A representative image is shown in Figure 1 and Online Video 1.

THE CAVOPULMONARY CONNECTION. There were 11 procedures in patients at a median age of 7.6 years (range 1.1 to 21.7 years) and weight of 22.5 kg (range 8.4 to 114.4 kg). Eight patients had undergone Fontan procedures, 2 bidirectional Glenns, and 1 a hemi-Fontan operation. The median fluoroscopy time was 44.2 min (range 15.2 to 119.5 min) with a mean total case contrast volume of 4.0 ± 1.8 ml/kg and mean contrast volume for ACT of 1.2 ± 0.4 ml/kg. During ACT, contrast was injected in the superior vena cava for superior cavopulmonary connections (CPC) and in the Fontan baffle or conduit for those with a completed Fontan, with an X-ray delay of 0.5 to 1 s. Representative images are shown in Figure 2 and Online Video 2.

THE PULMONARY VEINS. There were 5 patients at a median age of 3.5 years (range 0.4 to 14.2 years) and weight of 11.1 kg (range 5 to 50 kg) including 3 with pulmonary vein stenosis, 1 after prior correction of total anomalous pulmonary venous return, and 1 after a Senning procedure. The median fluoroscopy time was 29.8 min (range 16.5 to 84 min) with a mean total case contrast volume of 4.1 ± 1.6 ml/kg and mean contrast volume for ACT of 1.4 ± 0.4 ml/kg. During ACT, contrast was injected in the pulmonary arterial bed with an X-ray delay time up to 5 s depending on the best estimate of the pulmonary transit time.

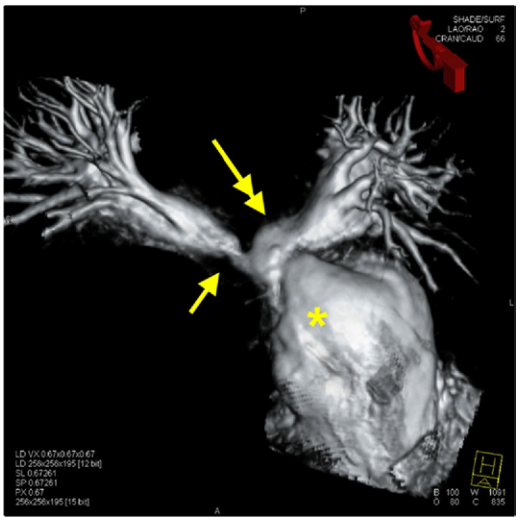

Figure 1. The Reconstructed RVOT and Central PA

A 3-dimensional reconstructed image from angiographic computed tomography of the right ventricular outflow tract (RVOT) and proximal central pulmonary arteries (PA) in a 2-year-old patient after surgical repair of tetralogy of Fallot. Image acquisition was performed during contrast injection through a catheter placed in the RVOT. The reconstructed image has been rotated to best portray the complex geometry of the distal main PA and proximal branch PAs. The icon in the **upper right-hand corner** of the figure shows the biplane camera angles needed to obtain the same view; **blue** indicates the angle is obtainable by standard biplane cineangiography, and **red** indicates not obtainable by standard biplane cineangiography. In this case, steep cranial angulation (66°) of the AP camera would be necessary, an angle not obtainable as indicated by the **red icon**. Easily apparent in this near-axial projection is severe proximal right PA stenosis **(single arrow)**. Also noted is the dilated main PA **(*)** after transannular patch and the acute origin of the left PA **(double-headed arrow)**. A complete rotation can be viewed in Online Video 1.

THE DISTAL PULMONARY ARTERIES. Four patients underwent ACT to evaluate distal pulmonary arteries (PAs) at a median age of 9.0 years (range 0.4 to 16.3 years) and weight of 26.9 kg (range 5 to 54.9 kg). Two had undergone unifocalization procedures, 1 a modified Blalock-Taussig shunt, and 1 had a stent fragment embolized to a distal PA. The median fluoroscopy time for cases was 71 min (range 42.3 to 102.3 min) with a mean total case contrast volume of 4.5 ± 1.5 ml/kg and mean contrast volume for ACT of 1.2 ± 0.3 ml/kg. During ACT, contrast was injected into the pulmonary arterial bed proximal to the area of interest with an X-ray delay time of 1 s. A representative image is shown in Figure 3 and Online Video 3.

MISCELLANEOUS OTHERS. Five other procedures were performed at a median age of 4.8 years (range 0.5 to 32 years) and weight of 16.1 kg (range 7.3 to 60.9 kg) in patients with the following diagnoses: patent ductus arteriosus, right ventricle to aorta, left superior vena cava to coronary sinus, pulmonary hypertension, and aortopulmonary collaterals (Fig. 4,

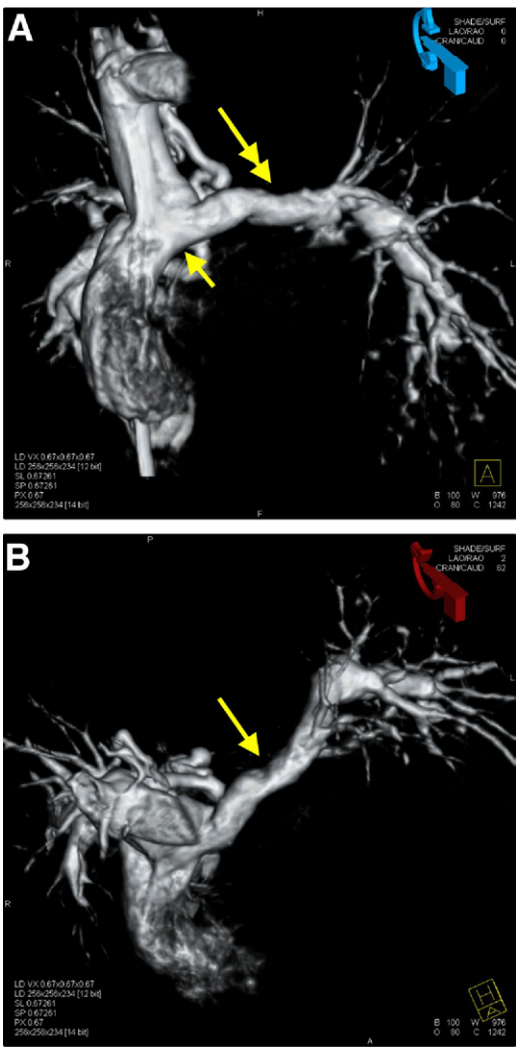

Figure 2. The CPC

(A) A 3-dimensional reconstructed image created from angiographic computed tomography of the Fontan pathway of a 5-year-old patient. Image acquisition occurred during contrast injection in the Fontan baffle. The image is viewed in a straight anteroposterior (AP) projection, similar to the view used for standard biplane cineangiography. The connection of the Fontan baffle to the superior vena cava **(single arrow)** and to the left pulmonary artery (PA) is well seen. There is some tortuosity of the left PA **(double-headed arrow)** and a suggestion of long-segment hypoplasia. **(B)** When the image is rotated to a steep cranial projection (62°), more significant narrowing of the left PA **(arrow)** in a front-to-back direction becomes apparent. As indicated by the **red icon** in the upper right corner, this view is not obtainable by standard biplane cineangiography. A complete rotation can be viewed in Online Video 2. CPC = cavopulmonary connection.

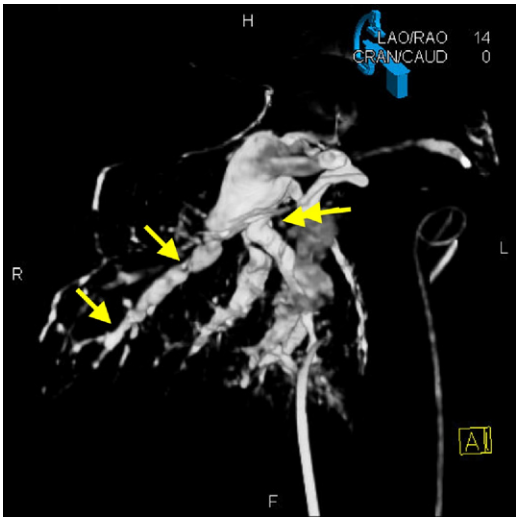

Figure 3. The Distal PA

A 3-dimensional reconstructed image from angiographic computed tomography of the right pulmonary artery (PA) of an 8.5-year-old patient after unifocalization of aortopulmonary collateral vessels to the right PA. Image acquisition was performed during contrast injection with the catheter positioned in the proximal right PA. The distal branching of the right PA is well seen, including multiple regions of distal stenoses **(single arrows)**. In addition, a collateral vessel unifocalized to the native right PA with its unnatural origin **(double-headed arrow)** is apparent. A complete rotation can be viewed in Online Video 3.

Online Video 4). The median fluoroscopy time was 17.2 min (range 1.7 to 46.4 min) with a mean total case contrast volume of 3.7 ± 2.4 ml/kg and mean contrast volume for ACT of 1.4 ± 0.7 ml/kg.

Image quality. Overall, diagnostic-quality images were obtained from ACT in 71% of cases (Table 2). In 19 of 41 total cases (46%), the ACT image was obtained instead of a standard cineangiogram, so a direct head-to-head comparison of ACT and cineangiogram quality could not be performed. In these cases, the reviewer subjectively determined whether the ACT was able to provide the diagnostic detail that could reasonably be expected from a standard cineangiogram. There was no statistically significant difference in the frequency of diagnostic-quality imaging across anatomic categories (Pearson chi-square = 2.2, p = NS). Further, univariate logistic regression failed to identify demographic, clinical, or procedural variables associated with obtaining diagnostic-quality images.

In 12 cases, the anatomic information obtained from ACT was felt to augment in a clinically meaningful way the information obtained from standard cineangiography. In 10 of these, ACT provided an improvement in relevant anatomic detail, including 7 cases of imaging the RVOT/central PAs (Fig. 1, Online Video 1) and 3 cases of imaging the CPC (Fig. 2, Online Video 2). In the majority of these cases, the relevant anatomic infor-

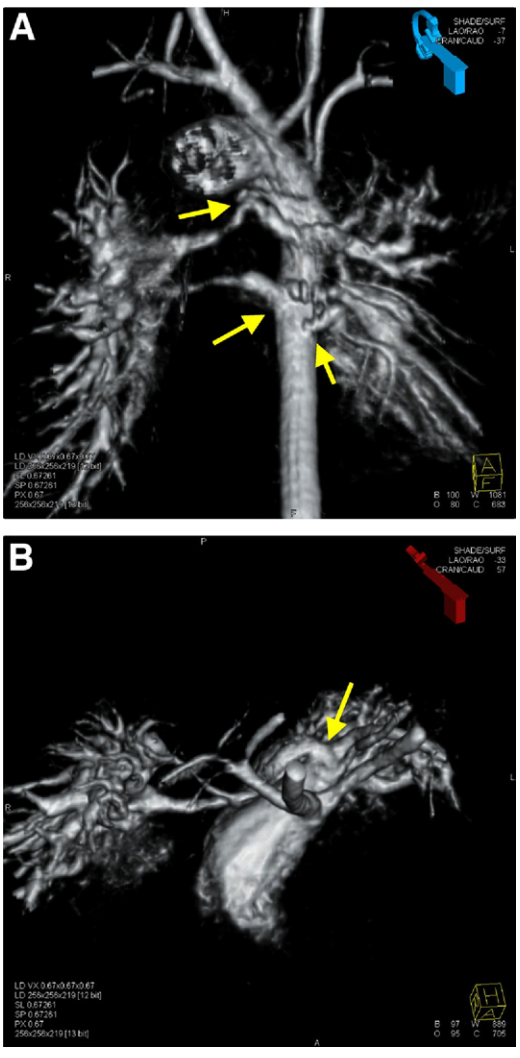

Figure 4. Aortopulmonary Collaterals

(A) A 3-dimensional reconstructed image from angiographic computed tomography of a 6-month-old patient with pulmonary atresia and major aortopulmonary collaterals. At least 3 collateral vessels are seen arising from the descending aorta **(arrows)** in this projection, which is an angle obtainable by standard biplane angiography as indicated by the **blue-colored icon** in the upper right-hand corner of the image. However, the origin of the most proximal collateral vessel from the aorta is not well seen, and direct catheter entry into this vessel was initially difficult. **(B)** When the image was rotated to a steep axial (57°) projection, it became evident that this collateral vessel arises quite posteriorly off of the proximal descending aorta **(arrow)**, knowledge that aided subsequent catheter entry into this vessel. This view is not obtainable by standard biplane angiography, as indicated by the **icon** in the right upper corner now being colored **red**. A complete rotation can be viewed in Online Video 4.

Table 2. Percentage (and Number) of ACT Studies Considered to Be of Diagnostic or Superior Image Quality, Separated by Anatomic Category

Anatomic Category	% Diagnostic (n/Total)*	% Superior (n/Total)*
RVOT/central pulmonary arteries	65% (13/20)	35% (7/20)
Cavopulmonary connection	82% (9/11)	27% (3/11)
Pulmonary veins	80% (4/5)	0% (0/5)
Distal pulmonary arteries	50% (2/4)	25% (1/4)
Other	80% (4/5)	20% (1/5)
Overall	71% (32/45)	27% (12/45)

*No significant difference in frequency across anatomic categories (p = NS). Abbreviations as in Table 1.

mation could only be obtained by rotating the 3D reconstructed image to an axial projection in order to fully delineate the anteroposterior contour of the vessel of interest. This is an imaging angle that cannot be achieved by standard cineangiography. In the remaining 2 cases, ACT imaging was able to aid in a complex catheter manipulation by overlaying the 3D reconstructed image onto the fluoroscopy screen. In 1 instance, this overlay facilitated cannulation of a unifocalized collateral vessel from the PA (Fig. 3, Online Video 3). In the other, it aided catheterization of an aortopulmonary collateral vessel from the posterior aspect of the descending aorta (Fig. 4, Online Video 4). There was no statistically significant difference in the frequency of superior-quality images across diagnostic categories (Pearson chi-square = 2.6, p = NS). Further, univariate logistic regression failed to identify demographic, clinical, or procedural variables associated with obtaining superior-quality images.

Radiation dose reduction. All radiation dose testing was performed after first increasing the kilovolt limit to 102 kVp to allow for copper filtration to be used during image acquisition at a higher kV range. The radiation exposure from various ACT programs as measured by the dose-area product ($\mu Gy \cdot m^2$) and the total effective dose (mSv, as estimated by dose calculation software) are summarized in Online Table 1. Variability in radiation dose from a single 5-s image acquisition sequence is based on patient size and the dose program selected, with estimated dose exposures ranging from <0.1 to 3.5 mSv. Our currently preferred ACT image acquisition program uses a dose of 0.17 μGy/frame and a frame rate of 60 frames/s. This results in similar radiation exposure as a comparable 5-s biplane cineangiogram across all phantom sizes (approximately 0.2 to 1.4 mSv) while maintaining image quality.

DISCUSSION

During our first year with ACT technology available in our pediatric cardiac catheterization laboratory, we performed ACT image acquisition in 41 procedures across a wide range of patient ages, sizes, and anatomic diagnoses. ACT technology was originally designed for application in interventional neuroradiology procedures (1–6,8). The technical details supporting this new technology have been well described (21–24). Its use has extended to other interventional radiology realms (9–14,16–18,25) and more recently into the adult cardiac electrophysiology suite (19). To our knowledge, this is the first report of the use of ACT technology in a cardiac catheterization laboratory for patients with congenital heart disease.

ACT provided diagnostic-quality imaging in over 70% of cases. The image quality from ACT has also proven to compare quite favorably with the current imaging standard in a variety of other arenas (7,16,26–31), although not all (15,32–34). In addition, in 12 cases, the information obtained from ACT augmented in a clinically meaningful way the information obtained from traditional angiography. In 10 patients, this included relevant anatomic information that was not attainable by standard angiography, typically complex geometric relations that are best viewed in an axial projection. In 2 other cases, ACT aided in complex catheter manipulations where the 3D ACT image was used as an overlay on the fluoroscopy screen.

The issue of radiation exposure is not entirely straightforward. The factory-installed default ACT programs result in substantial radiation exposure. However, we were able to reduce this to a more acceptable range through a number of efforts. First, we changed the kilovolt limit for all ACT programs to 102 kVp in order to allow for copper filtration to be used during image acquisition. Second, we removed the antiscatter grid for all subjects <15 kg. Third, we collimated top to bottom prior to image acquisition. Finally, we performed extensive testing of various dosing programs on phantoms to determine the optimal compromise between radiation exposure and image quality (Online Table 1). Currently, we find the best balance of image quality and radiation dose is achieved with the 0.17 μGy/frame dosing program at 60 frames/s. This results in a comparable radiation exposure to a 5-s biplane cineangiogram. The radiation exposure from clinical applications of ACT has not previously been reported. However, the exposure measured during our phantom testing is similar to that previously reported from 3D rotational angiography

(35) and from phantom testing of a similar C-arm CT system for neurovascular interventions (36). It is also well within the total estimated exposure during a routine pediatric cardiac catheterization (37–41). Finally, our measured exposure from ACT is significantly lower than the median exposure of 12 mSv for adult cardiac CT angiography in clinical use across 50 study sites recently reported by Hausleiter et al. (42).

We have identified a number of situations where ACT technology may be particularly suited. First, we have found it useful in providing additional anatomic detail of structures that are best visualized in axial projections. Not only has the reconstructed image been helpful, but we have also found a great deal of useful information in the tomographic volume sets that are generated (Fig. 5). Second, the use of the reconstructed 3D image from ACT as an overlay on the live fluoroscopy monitor may aid in complex catheter manipulations. Third, ACT may be useful to define the optimal camera angles prior to a planned intervention under standard biplane (or even single plane) fluoroscopic guidance. Finally, ACT may be useful when CT-quality soft-tissue imaging is desired in addition to the usual hemodynamic and anatomic information obtained at cardiac catheterization.

Regarding the technical aspects of performing an ACT, as a rule, we recommend diluting the contrast 1:2 with saline and administering a *contrast* volume of approximately 1.5 ml/kg during the duration of the injection. If the catheter is able to be positioned in close proximity to the area of interest, a 1-s X-ray delay setting should suffice. If the pulmonary veins are to be visualized following an injection in the pulmonary arteries, a longer X-ray delay will likely be needed. We currently favor the 5-s ACT program using a radiation dose of 0.17 μGy/frame and a frame rate of 60 frames/s. For extracardiac vascular structures, the ungated program with a breath-hold is sufficient.

We have identified a number of limitations to this imaging modality. First, the images obtained are time-averaged over the duration of the 5-s C-arm rotation. Thus, the temporal information obtained by standard angiography is not available with ACT. Second, we have had situations where there is "drop-out" of the signal in areas of very tight stenosis or adjacent to stented regions. Finally, we view the 3D reconstructed images with the same degree of skepticism that we have for the 3D images generated from standard CT or cardiac magnetic resonance (CMR). That is, a surface-rendered image such as these can be altered somewhat by the degree of windowing that occurs by the operator during post-processing. Thus, we are cautious about using the 3D images for precise measurements, instead using them for a more global appreciation of spatial relations.

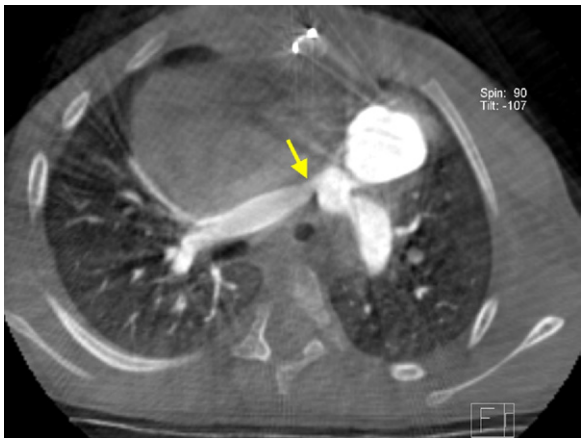

Figure 5. Two-Dimensional Slice from Tomographic Volume Set

An off-axis 2-dimensional axial image slice obtained from the complete tomographic volume set generated from angiographic computed tomography of a 2-year-old patient after surgical repair of tetralogy of Fallot. This volume set was used to generate the 3-dimensional reconstruction shown in Figure 1. In addition to the 3-dimensional image, there is a great deal of information contained in the 2-dimensional tomograms, which can be manipulated to view any plane in the volume set. In this view, the branching of the proximal pulmonary arteries (PA) is shown, with the severe stenosis of the proximal right PA (**arrow**). In addition, surrounding soft tissues are also visible as in traditional CT.

There are also limitations to the present study. First, this is a purely retrospective description of our early experience with this new modality in a relatively small number of cases. Second, the procedures during which ACT was used were selected by the operator with the hope that ACT would be a useful imaging technique for that particular anatomy. Thus, this likely represents a biased sampling of cases, the results of which may not necessarily generalize to other anatomic areas or to other operators. Third, determining the "diagnostic utility" of the images obtained involves a degree of subjectivity. Finally, this study focuses largely on the utility of the 3D images generated, with the understanding that there is also information to be obtained from the tomographic volume sets (Fig. 5).

Multislice spiral computed tomography (MSCT) is an alternative imaging modality by which detailed 3D cardiovascular anatomy can be obtained and has been used successfully in a variety of forms of congenital heart disease (43–45). However, in patients where invasive catheter study is indicated for diagnostic or therapeutic purposes, ACT may have advantages over conventional MSCT: 1) the images are easily obtainable without significantly prolonging the catheterization procedure; 2) the contrast dose for an ACT acquisition is less than or equal to that used

for MSCT; and 3) the generated images can be immediately and accurately registered with real-time fluoroscopy to serve as a 3D overlay roadmap in the cardiac catheterization laboratory. A more intriguing alternative to ACT for use in the catheterization laboratory is CMR fused with X-ray. Although CMR requires a substantially longer image acquisition time than ACT, there is no ionizing radiation and the functional information obtained by CMR is available. Several investigators have described techniques for the registration of CMR images with biplane fluoroscopy to allow the use of this 3D dataset for roadmapping (46–49). Much future work will be required to determine the optimal application of these new strategies in transcatheter evaluation and treatment of congenital heart disease.

CONCLUSIONS

ACT is a new imaging modality available in the pediatric cardiac catheterization laboratory that provides a complete volume set of contrast-enhanced CT images from a single C-arm rotation. The images, including a 3D reconstruction, can be quickly generated and used in real time during the procedure. We have found that this technique is able to provide diagnostic-quality imaging in over 70% of cases. Further experience will likely only increase this percentage. ACT may provide additional clinically relevant data in situations where an axial projection is needed to best view the area of interest, such as the reconstructed RVOT and the CPC. The 3D images obtained by ACT can also be used to set the ideal camera angles for further angiography or intervention. Further, the 3D images can be used as an image overlay on the live fluoroscopy screen to aid with complex catheter manipulations. With the appropriate technical modifications, the contrast and radiation exposure from ACT can be comparable to a standard biplane cineangiogram. Further work is needed to continue to optimize the technical aspects and define the clinical utility of this new modality.

Acknowledgment

The authors thank Marily Sarmiento, Siemens Medical Solutions, for technical assistance.

Reprint requests and correspondence: Dr. Andrew C. Glatz, Division of Cardiology, 6th Floor Main Building, The Children's Hospital of Philadelphia, 34th Street and Civic Center Boulevard, Philadelphia, Pennsylvania 19104. *E-mail: glatz@email.chop.edu.*

REFERENCES

1. Benndorf G, Klucznik RP, Strother CM. Angiographic computed tomography for imaging of underdeployed intracranial stent. Circulation 2006; 114:E499–500.
2. Benndorf G, Claus B, Strother CM, Chang L, Klucznik R. Increased cell opening and prolapse of struts of a neuroform stent in curved vasculature: value of angiographic computed tomography: technical case report. Neurosurgery 2006;58 (suppl 2):ONS-380–1.
3. Buhk JH, Lingor P, Knauth M. Angiographic CT with intravenous administration of contrast medium is a noninvasive option for follow-up after intracranial stenting. Neuroradiology 2008;50:349–54.
4. Engelhorn T, Struffert T, Richter G, et al. Flat panel detector angiographic CT in the management of aneurysmal rupture during coil embolization. AJNR Am J Neuroradiol 2008;29: 1581–4.
5. Gupta V, Chugh M, Walia BS, Vaishya S, Jha AN. Digital subtraction angiography laboratory with inbuilt CT (DynaCT): application during intracranial anurysm embolization. Neurol India 2008;56:90–1.
6. Heran NS, Song JK, Mamba K, Smith W, Niimi Y, Berenstein A. The utility of DynaCT in neuroendovascular procedures. AJNR Am J Neuroradiol 2006;27:330–2.
7. Jou LD, Mohamed A, Lee DH, Mawad ME. 3D rotational digital subtraction angiography may underestimate intracranial aneurysms: Findings from two basilar aneurysms. AJNR Am J Neuroradiol 2007;28: 1690–2.
8. Richter G, Engelhorn T, Struffert T, et al. Flat panel detector angiographic CT for stent-assisted coil embolization of broad-based cerebral aneurysms. AJNR Am J Neuroradiol 2007; 28:1902–8.
9. Biasi L, Ali T, Hinchliffe R, Morgan R, Loftus I, Thompson M. Intraoperative DynaCT detection and immediate correction of a type 1a endoleak following endovascular repair of abdominal aortic aneurysm. Cardiovasc Intervent Radiol 2009;32:535–8.
10. Binkert CA, Alencar H, Singh J, Baum RA. Translumbar type II endoleak repair using angiographic CT. J Vasc Interv Radiol 2006;17:1349–53.
11. Georgiades CS, Hong K, Geschwind JF, et al. Adjunctive use of C-arm CT may eliminate technical failure in adrenal vein sampling. J Vasc Interv Radiol 2007;18:1102–5.
12. Irie K, Murayama Y, Saguchi T, et al. DynaCT soft-tissue visualization using an angiographic c-arm system: initial clinical experience in the operating room. Neurosurgery 2008;63: 266–72.
13. Kim HC, Chung JW, An S, et al. Left inferior phrenic artery feeding hepatocellular carcinoma: angiographic anatomy using C-arm CT. AJNR Am J Neuroradiol 2009;193:W288–94.
14. Kim HC, Chung JW, Park JH, et al. Transcatheter arterial chemoembolization for hepatocellular carcinoma: prospective assessment of the with C-arm CT. J Vasc Interv Radiol 2009; 20:888–95.
15. Meyer BC, Frericks BB, Voges M, et al. Visualization of hypervascular liver lesions during TACE: comparison of angiographic C-arm CT and MDCT. AJR Am J Roentgenol 2008;190: W263–9.
16. Meyer BC, Witschel M, Frericks BB, et al. The value of combined soft-tissue and vessel visualisation before transarterial chemoembolisation of the liver using C-arm computed tomography. Eur Radiol 2009;19:2302–9.

17. Virmani S, Ryu RK, Sato KT, et al. Effect of C-arm angiographic CT on transcatheter arterial chemoembolization of liver tumors. J Vasc Interv Radiol 2007;18:1305–9.
18. Wallace MJ. C-arm computed tomography for guiding hepatic vascular interventions. Tech Vasc Interv Radiol 2007;10:79–86.
19. Nolker G, Gutleben KJ, Marschang H, et al. Three-dimensional left atrial and esophagus reconstruction using cardiac C-arm computed tomography with image integration into fluoroscopic views for ablation of atrial fibrillation: accuracy of a novel modality in comparison with multislice computed tomography. Heart Rhythm 2008;5:1651–7.
20. Biasi L, Ali T, Thompson M. Intraoperative dynaCT in visceral-hybrid repair of an extensive thoracoabdominal aortic aneurysm. Eur J Cardiothorac Surg 2008;34:1251–2.
21. Fahrig R, Fox AJ, Lownie S, Holdsworth DW. Use of a C-arm system to generate true three-dimensional computed rotational angiograms: preliminary in vitro and in vivo results. AJNR Am J Neuroradiol 1997;18:1507–14.
22. Fahrig R, Dixon R, Payne T, Morin RL, Ganguly A, Strobel N. Dose and image quality for a cone-beam C-arm CT system. Med Phys 2006;33:4541–50.
23. Gupta R, Grasruck M, Suess C, et al. Ultra-high resolution flat-panel volume CT: fundamental principles, design architecture, and system characterization. Eur Radiol 2006;16:1191–205.
24. Lauritsch G, Boese J, Wigstrom L, Kemeth H, Fahrig R. Towards cardiac C-arm computed tomography. IEEE Trans Med Imag 2006;25:922–34.
25. Meyer BC, Frericks BB, Albrecht T, Wolf KJ, Wacker FK. Contrast-enhanced abdominal angiographic CT for intra-abdominal tumor embolization: a new tool for vessel and soft tissue visualization. Cardiovasc Intervent Radiol 2007;30:743–9.
26. Benndorf G, Strother CM, Claus B, et al. Angiographic CT in cerebrovascular stenting. AJNR Am J Neuroradiol 2005;26:1813–8.
27. Eide KR, Odegard A, Myhre HO, Lydersen S, Hatlinghus S, Haraldseth O. DynaCT during EVAR: a comparison with multidetector CT. Eur J Vasc Endovasc Surg 2009;37:23–30.
28. Hiu T, Kitagawa N, Morikawa M, et al. Efficacy of DynaCT digital angiography in the detection of the fistulous point of dural arteriovenous fistulas. AJNR Am J Neuroradiol 2009;30:487–91.
29. Iwazawa J, Ohue S, Mitani T, et al. Identifying feeding arteries during TACE of hepatic tumors: comparison of C-arm CT and digital subtraction angiography. AJR Am J Roentgenol 2009;192:1057–63.
30. Singh J, Carrino JA, Alencar H, Binkert CA. Comparison of angiographic CT and spiral CT to assess cement distribution after vertebral augmentation. J Vasc Interv Radiol 2007;18:1547–51.
31. Wallace MJ, Murthy R, Kamat PP, et al. Impact of C-arm CT an hepatic arterial interventions for hepatic malignancies. J Vasc Interv Radiol 2007;18:1500–7.
32. Baumann C, Fuchs H, Westphalen K, Hierholzer J. Detection of cement leakage after vertebroplasty with a non-flat-panel angio unit compared to multidetector computed tomography: an ex vivo study. Cardiovasc Intervent Radiol 2008;31:1222–7.
33. Buhk JH, Elolf E, Jacob D, Rustenbeck HH, Mohr A, Knauth M. A comparison of angiographic CT and multisection CT in lumbar myelographic imaging. AJNR Am J Neuroradiol 2008;29:442–6.
34. Buhk JH, Kallenberg K, Mohr A, Dechent P, Knauth M. Evaluation of angiographic computed tomography in the follow-up after endovascular treatment of cerebral aneurysms-a comparative study with DSA and TOF-MRA. Eur Radiol 2009;19:430–6.
35. Bridcut RR, Murphy E, Workman A, Flynn P, Winder RJ. Patient dose from 3D rotational neurovascular studies. Br J Radiol 2007;80:362–6.
36. Daly MJ, Siewerdsen JH, Moseley DJ, Jaffray DA, Irish JC. Intraoperative cone-beam CT for guidance of head and neck surgery: assessment of dose and image quality using a C-arm prototype. Med Phys 2006;33:3767–80.
37. Axelsson B, Khalil C, Lidegran M, Schuwert P, Mortensson W. Estimating the effective dose to children undergoing heart investigations: a phantom study. Br J Radiol 1999;72:378–83.
38. Bacher K, Bogaert E, Lapere R, De Wolf D, Thierens H. Patient-specific dose and radiation risk estimation in pediatric cardiac catheterization. Circulation 2005;111:83–9.
39. Boothroyd A, McDonald E, Moores BM, Sluming V, Carty H. Radiation exposure to children during cardiac catheterization. Br J Radiol 1997;70:180–5.
40. Li LB, Kai M, Kusama T. Radiation exposure to patients during paediatric cardiac catheterisation. Radiat Prot Dosimetry 2001;94:323–7.
41. Rassow J, Schmaltz AA, Hentrich F, Streffer C. Effective doses to patients from paediatric cardiac catheterization. Br J Radiol 2000;73:172–83.
42. Hausleiter J, Meyer T, Hermann F, et al. Estimated radiation dose associated with cardiac CT angiography. JAMA 2009;301:500–7.
43. Kim TH, Kim YM, Suh CH, et al. Helical CT angiography and three-dimensional reconstruction of total anomalous pulmonary venous connections in neonates and infants. AJR Am J Roentgenol 2000;175:1381–6.
44. Goo HW, Park IS, Ko JK, Kim YH, Seo DM, Park JJ. Computed tomography for the diagnosis of congenital heart disease in pediatric and adult patients. Int J Cardiovasc Imag 2005;21:347–65.
45. Jelnin V, Co J, Muneer B, Swaminathan B, Toska S, Ruiz CE. Three dimensional CT angiography for patients with congenital heart disease: scanning protocol for pediatric patients. Catheter Cardio Int 2006;67:120–6.
46. Ratnayaka K, Raman VK, Faranesh AZ, et al. Antegrade percutaneous closure of membranous ventricular septal defect using x-ray fused with magnetic resonance imaging. J Am Coll Cardiol Intv 2009;2:224–30.
47. Rhode KS, Hill DLG, Edwards PJ, et al. Registration and tracking to integrate x-ray and MR images in an XMR facility. IEEE T Med Imaging 2003;22:1369–78.
48. Gutierrez LF, de Silva R, Ozturk C, et al. Technology preview: x-ray fused with magnetic resonance during invasive cardiovascular procedures. Catheter Cardio Int 2007;70:773–82.
49. de Silva R, Gutierrez LF, Raval AN, McVeigh ER, Ozturk C, Lederman RJ. X-ray fused with magnetic resonance imaging to target endomyocardial injections: validation in a swine model of myocardial infarction. Circulation 2006;114:2342–50.

Key Words: angiographic computed tomography ■ cardiac catheterization ■ congenital heart disease.

APPENDIX

For a supplemental figure, table, and videos, please see the online version of this article.